Flexibility within the Heads of Muscle Myosin-2 Molecules

Neil Billington[1,†], **Derek J. Revill**[1], **Stan A. Burgess**[1], **Peter D. Chantler**[2] and **Peter J. Knight**[1]

*1 - **School of Molecular and Cellular Biology and Astbury Centre for Structural Molecular Biology,** University of Leeds, Leeds LS2 9JT, UK*
*2 - **Unit of Molecular and Cellular Biology,** Royal Veterinary College, University of London, Royal College Street, London NW1 0TU, UK*

Correspondence to Peter J. Knight: *School of Molecular and Cellular Biology, LC Miall Building, University of Leeds, Leeds LS2 9JT, UK. p.j.knight@leeds.ac.uk*
http://dx.doi.org/10.1016/j.jmb.2013.11.028
Edited by R. Craig

Abstract

We show that negative-stain electron microscopy and image processing of nucleotide-free (apo) striated muscle myosin-2 subfragment-1 (S1), possessing one light chain or both light chains, is capable of resolving significant amounts of structural detail. The overall appearance of the motor and the lever is similar in rabbit, scallop and chicken S1. Projection matching of class averages of the different S1 types to projection views of two different crystal structures of apo S1 shows that all types most commonly closely resemble the appearance of the scallop S1 structure rather than the methylated chicken S1 structure. Methylation of chicken S1 has no effect on the structure of the molecule at this resolution: it too resembles the scallop S1 crystal structure. The lever is found to vary in its angle of attachment to the motor domain, with a hinge point located in the so-called pliant region between the converter and the essential light chain. The chicken S1 crystal structure lies near one end of the range of flexion observed. The Gaussian spread of angles of flexion suggests that flexibility is driven thermally, from which a torsional spring constant of ~23 pN·nm/rad^2 is estimated on average for all S1 types, similar to myosin-5. This translates to apparent cantilever-type stiffness at the tip of the lever of 0.37 pN/nm. Because this stiffness is lower than recent estimates from myosin-2 heads attached to actin, we suggest that binding to actin leads to an allosteric stiffening of the motor–lever junction.

Introduction

The mechanical properties of muscle crossbridges underlie muscle function but are controversial [1–4]. The swinging lever hypothesis of muscle contraction envisages that the relative movements of the thick and thin filaments originate from the part of the actomyosin crossbridge that is furthest from the actin filament, acting as a lever. This lever amplifies the conformational change driven by ATP hydrolysis within the core of the myosin motor leading to mutual filament sliding [5]. In muscle shortening against a load, force is produced in addition to shortening; the characteristics of the work produced depend on the mechanical properties of the active crossbridge. These properties are still disputed despite decades of ingenious study and despite their importance for understanding the general principles of motor protein function. In part, this is because the speed and dynamic nature of the crossbridge cycle and the complexity of the contractile apparatus make unambiguous interpretation of ensemble properties difficult. We have therefore sought to understand the mechanical properties of the crossbridge by direct observation of individual myosin heads.

Striated muscle myosins are members of the myosin-2 branch of the myosin phylogenetic tree [6,7] and share a common structural plan. Twin 230-kDa heavy chains each form a motor domain (MD), then continue as an extended α-helix originally named the "lever arm" [8], but here named more concisely the lever before uniting to form a parallel, in-register, α-helical, coiled-coil tail. The MD plus lever is generally referred to as the myosin head or subfragment-1 (S1). The lever helix is stabilised by two calmodulin-like, bi-lobed light chains: an essential

light chain (ELC) adjacent to the MD followed by a regulatory light chain (RLC). The ELC binds because it recognises a canonical IQ motif [9] in the lever helix, while the RLC recognises a modified IQ motif in which a distal WxWW sequence produces a sharp kink in the lever helix [10]. All myosin-2s have the same length of lever, with the IQ motifs always the same distance from the MD and the tail and the same distance apart (the I residues of the IQ motifs are 26 amino acid residues apart). It is therefore expected that all myosin-2 heads share a common structure, though their enzymatic and mechanical properties will depend on the specific amino acid sequences of the heavy and light chains.

Electron microscopy (EM) has advantages over X-ray crystallography in defining molecular flexibility. Although crystallography has produced a wealth of structural detail regarding the myosin-2 head, it has limitations: progress can be slow because crystal formation is capricious, and desired conformers may not crystallise; more fundamentally, flexibility is necessarily suppressed within a crystal. By contrast, EM allows rapid throughput of samples and can indicate the range of conformations present in solution at the point of fixation, albeit at lower resolution. EM, when combined with image processing to improve the signal-to-noise ratio of the data, provides a link between high-resolution structural studies of individual conformations and data from solution studies regarding the structural dynamics of the protein [11]. This approach has been used to interpret tomograms of rigor insect flight muscle and has shown that distortions in the lever region of the S1 crystal structure have to be made to fit it into the EM density map, especially when the muscle is stretched [12].

X-ray crystallography has revealed some diversity of structures of the lever of myosin-2 heads. Through comparisons between different crystal structures, some sites of flexibility have been discerned [13,14]. In particular, a site in the heavy chain at the junction between the MD and the lever is a straight helix in many structures but distorted in others, leading to its description as a pliant region and the proposal that it could play a role in crossbridge elasticity [14]. Also, the shape and position of the lever appear to differ between heads from different myosins in equivalent nucleotide states [10,14–16]. It is not known whether such differences represent true structural differences between the myosins in solution or whether they arise simply because of the different crystallisation conditions used, which may select particular structures from a dynamic range of conformations that are similarly populated by these different myosins in solution. In the compactly folded and shutdown conformer of scallop myosin, the closer resemblance of its lever to that seen in the crystal structure of chicken skeletal myosin rather than scallop striated muscle myosin [17] argues for the latter alternative.

Previous work in our group used negative-stain EM and single particle image processing on whole myosin molecules to show that flexibility exists within the heads [11,18]. The range of shapes seen was greater than expected given the high stiffness that has been estimated for crossbridges in muscle (see Ref. [19]), raising a question concerning the degree of distortion that each molecule undergoes when drying in stain during specimen preparation. However, measurement of myosin tail stiffness from the quantitative analysis of the diversity among such EM images [20] provided a similar value to solution studies [21], suggesting that negative-stain EM produces images that do represent the situation in solution. The stiffness of a macromolecule can be estimated by quantitative analysis of a set of images because the breadth of the distribution of shapes is inversely related to stiffness through the Equipartition theorem [22]. The ergodic hypothesis states that the set of images can be either of one molecule changing shape over time or (as here) single images of many molecules.

In dissecting the problem of crossbridge stiffness in muscle, it is important to know what degree of flexibility and elasticity exists within the heads themselves, when unconnected to the tail. For this reason, we have here investigated S1 rather than whole myosin molecules, using negative-stain EM and image processing. The use of S1 also avoids any lingering concerns that other parts of the whole molecule might create distorting forces during specimen preparation. It also avoids a problem associated with processing images of double-headed myosin, namely, that the two heads do not maintain a fixed relationship to each other and this added variability can hamper image alignment.

We have compared the appearances in EM of several S1 species, using negative staining since myosin-2 S1 is too small (~130 kDa) to identify by unstained cryo-EM. Scallop and chicken striated muscle S1s were imaged to allow direct comparison with existing crystal structures (PDB IDs: 1SR6/2OS8 and 2MYS, respectively). We also studied rabbit skeletal muscle S1, which is enzymatically well characterised but has not yet been crystallised. Indeed, there is no crystal structure of any mammalian myosin-2 head to date, making it important to determine how closely such myosins resemble those crystal structures that have been determined. We also studied the effect of reductive methylation on the structure of chicken S1 since this chemical modification was used to crystallise it. In particular, we wished to determine whether the differences in lever shape between crystal structures of scallop and chicken S1s are a genuine species difference or are instead a consequence of either methylation or crystallisation.

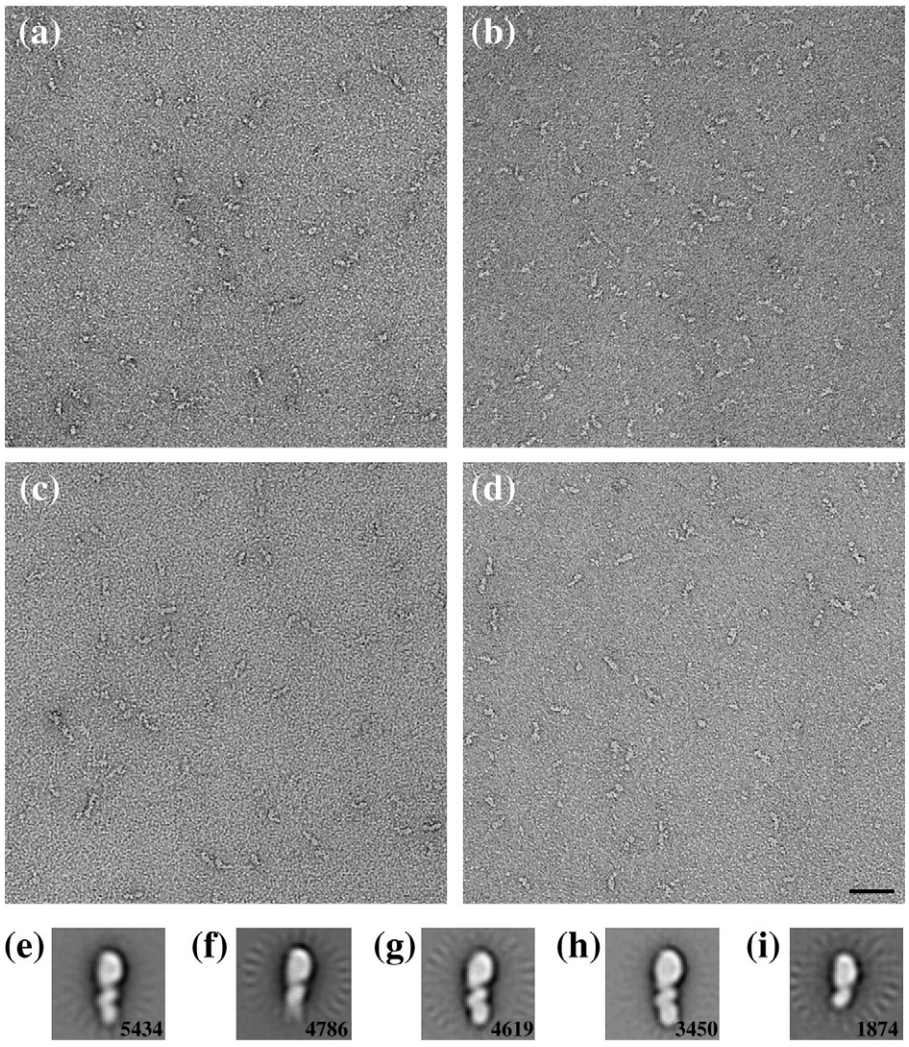

Fig. 1. Fields of view and global image averages of different types of myosin-2 S1.(a–d) Areas of raw micrographs of four different types of full-length myosin-2 S1. The scale bar represents 50 nm. (e–i) Global image averages resulting from alignment of multiple images of each S1 type. (a and e) RbS1. (b and f) ScS1. (c and g) CkS1. (d and h) mCkS1. (i) rabbit skeletal chymotryptic S1 (A1 ELC). Numbers in (e)–(i) show the number of particles in each dataset. Side length of image average panels is 31.2 nm.

Results

Features of four types of myosin-2 S1 in negative stain

To compare the structures of myosin-2 heads from several sources, we negatively stained each type in the absence of nucleotide then examined it by EM. We compared S1s containing both ELC and RLC prepared by papain proteolysis of rabbit skeletal muscle myosin (RbS1), scallop cross-striated adductor muscle myosin (ScS1), chicken skeletal muscle myosin (CkS1) and CkS1 that had been reductively methylated (mCkS1). We found that, in each case, the S1 molecules adsorbed to the carbon film in a similar way to the heads of intact myosin: the long axis typically lay in the plane of the carbon and there was a strong preference for a particular side of the molecule to adsorb. Moreover, the motor and lever domains could often be distinguished in raw micrographs of the negatively stained S1s, as found previously for intact myosin (Fig. 1a–d) [18,23]. Consequently, a reliable computational alignment of individual S1 by single particle methods was readily accomplished; even in the global averages, some subdomain features of the MD and the two bound light chains of the lever (ELC and RLC) are apparent (Fig. 1e–g). In particular, the MD shows the resemblance to a human head in profile previously noted in myosin-2 and myosin-5a [18,24] in which the human is facing left. The close similarity of Fig. 1h to

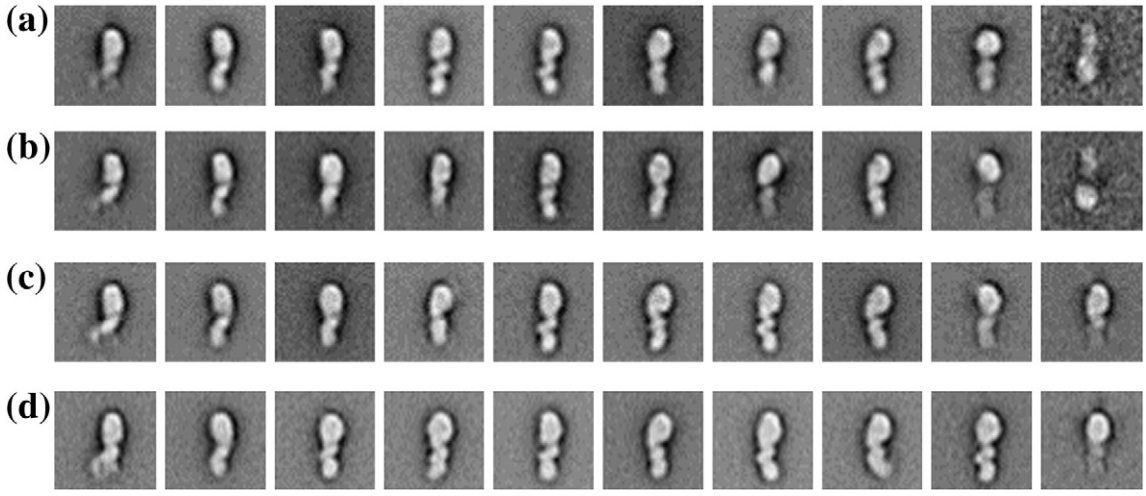

Fig. 2. Range of appearances of nucleotide-free S1 from different sources.Each row of the montage shows the result of K-means clustering of all the particles of an aligned dataset into 10 classes. Classes have been rearranged along the row to show the general similarities between the four datasets when compared down a column. (a) RbS1; (b) ScS1; (c) CkS1; (d) mCkS1. Note in (a) and (b), the rightmost panels show that a small fraction of the S1s have misaligned upside down and have formed a small separate class. Side length of all image panels is 31.2 nm.

Fig. 1g indicates that methylation of almost all the lysine side chains of CkS1 [25] has no effect on its behaviour as a specimen for negative staining.

To determine whether the overall shape of S1 and its orientation on the carbon film was governed by the RLC, we also imaged and aligned rabbit skeletal S1 that had been truncated after the ELC by chymotryptic proteolysis [26]. The overall appearance and orientation of the truncated molecule was similar to the corresponding regions in class averages of the myosin S1 molecule digested by papain (Fig. 1i compared to Fig. 1e). This shows that removal of the C-terminal part of the lever, including the associated RLC, does not produce a large structural change in the remainder of the molecule. It also shows that it is possible to reliably image and align this small head fragment (~110 kDa total mass).

Classification of the particles from the four different full-length S1s shows that, despite the detail in the global average, there is nevertheless a (limited) range of appearances of both MD and light chains present in each of the datasets (Fig. 2). The different appearances are remarkably similar between the different S1s. In many cases, individual subdomains can be recognised within the S1 and in greater detail than in the global average, as is expected for well-aligned particles of diverse appearance. The N- and C-lobes of the ELC are clearly resolved in some averages. The RLC is a strong feature of more classes than was the case with heads of intact myosin [18], probably because of the absence of the tail and other head that complicate the head–tail junction of intact myosin. Nevertheless, the RLC in S1 appears as an ellipse oriented along the lever axis rather than as two lobes obliquely crossing it, which is also the result expected from its different arrangement, grasping the hook in the heavy chain lever helix [10,13]. The RLC is a weaker feature in the global average of ScS1 (Fig. 1f) than the other S1s, and the classification (Fig. 2) correspondingly shows more classes for ScS1 that have a weak RLC feature, presumably because the RLC is easily lost from ScS1 preparations.

It is apparent from Fig. 2 that some S1 molecules appear straight while others curve to the left or to the right. Since EM and crystallography have shown that myosin-2 heads are inherently curved, largely in a single plane [10,27,28], there are two possible classes of explanation for this diversity of shape. First, the molecules may adsorb to the carbon film in a variety of orientations, yielding varying shapes in the projection view recorded by EM; second, they may be inherently flexible. To distinguish between these alternatives, we analysed the data further by grouping together particles displaying the same MD features, in order to test whether there was still the variation in shape that would imply flexibility within such groups having a given orientation. Such analyses work best with large datasets. Given the similarities of the four datasets shown in Fig. 2, we pooled all four datasets, keeping track of which particles were from each individual dataset so that we could subsequently determine whether there were systematic differences between them.

Comparison of different types of full-length S1

Pooling all four S1 datasets (RbS1, ScS1, CkS1 and mCkS1) and realigning the images produces a global average similar to those of each separate dataset, as expected (Fig. 3a). Classification of the

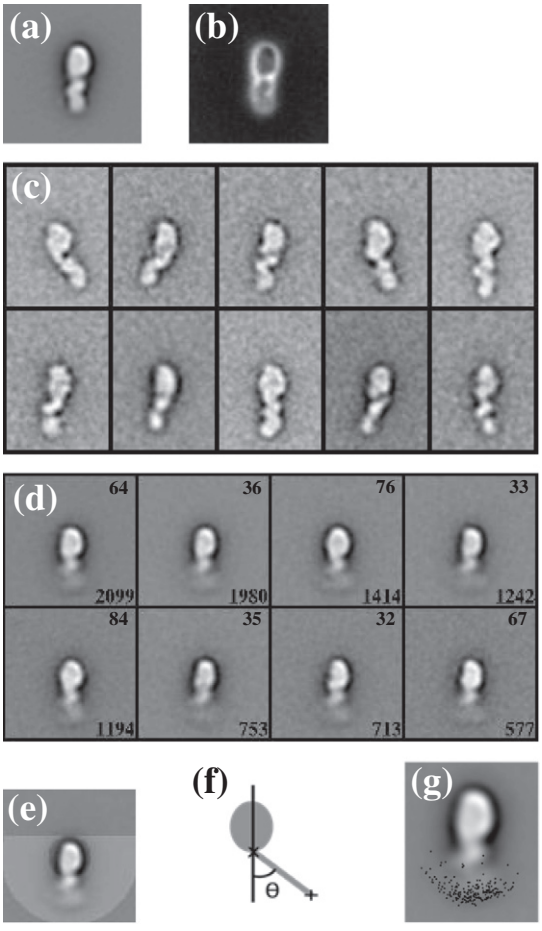

Fig. 3. Co-alignment and co-classification of multiple myosin S1 datasets.(a) Global average and (b) global variance images resulting from alignment of 17,307 images of S1 from RbS1, ScS1, CkS1 and mCkS1. In (b), white indicates high variance. (c) Class averages after further alignment of MD alone in each average against the global average MD. These 10 examples (from 400 classes) are selected to show that class averages with differing appearances became aligned with the long axis of the MD vertical. (d) Eight classes from classification into 100 classes according to the MD appearance, using hierarchical ascendant classification. These are the largest classes, each containing >500 particles; they include 57.6% of the combined data and were selected for further analysis. Arbitrary class number top right; number of particles at lower right. (e) The semi-annular mask used to classify the levers, superimposed (in paler grey) on the global average resulting from alignment of the MD. (f) How the lever angle for each class (θ) was measured relative to the vertical axis of the MD by marking the tip of the lever (+) and using the MD–lever junction as marked in the global average of the combined data (×). Lever tips to the left of the MD–lever junction were assigned negative angles. (g) The marked positions of the tips of levers after lever classification (black dots) superposed on the global average. Side length in (a)–(e) is 41.6 nm; in (g), it is 30.9 nm.

aggregated data into a large number of classes allows the full diversity of appearances to be apparent with improved signal to noise compared to raw images. Images from each S1 dataset are spread across these averages, rather than segregating into distinct classes, which indicates that systematic differences between the datasets are small compared to the variations within each dataset. These class averages contain improved MD detail so that the MD features alone of each class average could be computationally aligned with the MD long axis vertical within the viewing window (Fig. 3c), and this realignment caused the levers to become spread away from the vertical. To group together molecules with the same MD appearance, we then reclassified the MD-aligned stack of raw images using only features within the MD. The eight most abundant appearances of the MD (among 100 classes) are shown in Fig. 3d, from which it is apparent that there is close similarity of most members in this group to the global average. Thus, many S1 molecules are seen in the same MD view, allowing lever position relative to the MD to be explored.

To quantitate the range of lever positions, we classified the full stack of MD-aligned images into 200 classes using only features in the lever region (Fig. 3e), and we then measured the lever angle of each class relative to the long axis of the MD by locating the position of the tip of the lever in each class average (Fig. 3f). The spread of lever tip positions (Fig. 3g) is concentrated in an arc that is densest near its centre. This is the behaviour expected for a thermally excited elasticity between MD and lever tip that could arise from bending along the lever and/or flexibility at the MD–lever junction. However, as noted above, it could in principle also arise from a range of molecular orientations on the carbon film without flexibility. However, as a result of the MD classification of the same image stack, each individual particle could be assigned to an MD class and a lever angle class. The distributions of lever angle for any MD class could therefore be determined, and these distributions for each of the four S1 types could also be compared. We focused further analyses on the eight MD classes that were the most abundant.

Lever angle distributions for the two most highly populated MD classes are shown in Fig. 4. They are displayed using percentage cumulative frequency plots rather than histograms. We chose this display because such plots show every individual data point rather than the arbitrary bins used in histograms and, thus, show the data more objectively, and they are better able to display multiple datasets where differences between them are small. In these percentage cumulative frequency plots, the fitted Gaussian curves show as sigmoid lines, which cross the 50% value at the mean fitted lever angle. It is apparent that all four types of S1 show a very similar extent of lever angle variation, and it is described

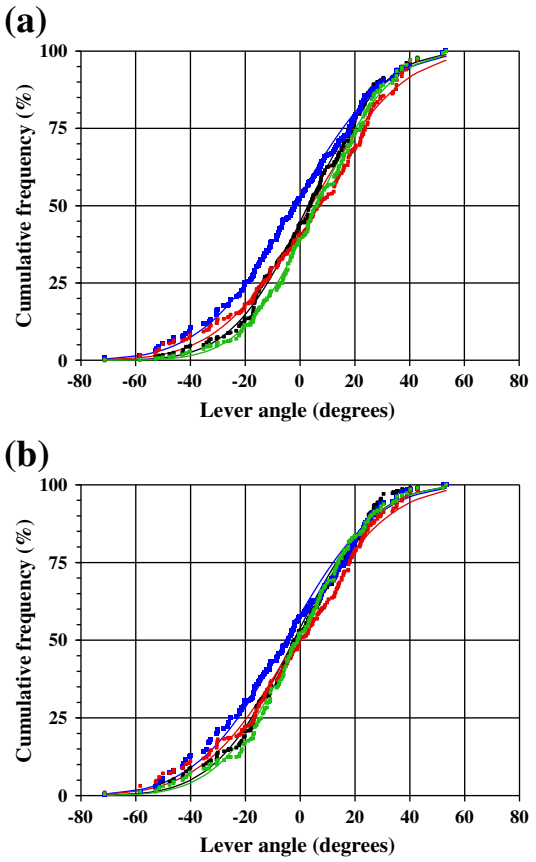

Fig. 4. Lever angle distributions of MD classes.(a) MD class 64 (2,099 particles); (b) MD class 36 (1,980 particles). Panels show data points for every image within an MD class, segregated by S1 type and arranged in order of ascending lever angle. RbS1, red; ScS1, blue; CkS1, green; mCkS1, black. Smooth lines of the same colours are Gaussian best fits to each set of data.

well by a Gaussian spread. The mean lever angles for the four types are all close to 0°, with ScS1 tending to angle a few degrees more to the left. Averaged over all eight MD classes, the mean angles are as follows: RbS1, −1.1°; ScS1, −5.2°; CkS1, −0.8°; mCkS1, +1.1° (see detailed breakdown in Table 1). MD class 35 looks the least similar to the typical head-in-profile appearance (Fig. 3d), indicating that the S1 is viewed from a different angle. Correspondingly, the mean lever angles are generally shifted to lower values but the differences between the S1 types remain similar (Table 1). Because of the large numbers of particles measured, the differences in lever angle distributions between S1 types in many MD classes reach statistical significance, but the differences are small.

To observe the variations in structure of S1 between and within the major MD classes, we made a set of five image averages for each type of S1 in each MD class, each average containing 20% of the angle-sorted data. Because the first and the last averages contain a wider range of the lever angle distribution, the levers are more smeared out than in the central average that covers only a narrow angular range. Figure 5a and b shows the same MD classes shown in Fig. 4. The averages show that the substructures of the S1 types are similar to one another in the central averages and display altered shapes in similar ways when the lever is angled differently. Importantly, they confirm that the change in lever angle is not accompanied by a change in MD orientation or appearance, reinforcing the conclusion that S1 is flexible. The major conclusion, therefore, is that S1 shows flexibility in its shape. All four S1 types are very similar to one another, both in the mean angle displayed between motor and lever and in the amount of variation in lever angle present.

Flexibility of S1

To determine the sites of flexibility within S1, we subdivided the 2,099 images in the most abundant MD class (Fig. 3d; head-in-profile appearance) into 10 or 20 classes based on lever angle (Fig. 5c or SI Movie 1, respectively). Inspection of the classes shows that the levers change little in shape or substructure; for instance, the two-lobed appearance of the ELC can be resolved in several classes. This indicates that the lever itself is relatively stiff. Instead, SI Movie 1 indicates that a major site of flexibility is at the junction between the MD and the lever. To determine the location of this site more objectively, for each class, we drew a straight line through the lever from its tip to its junction with the MD and extrapolated it across the MD. The coordinates were calculated of every intersection of each line with every other line (shown as a scatter plot in Fig. 5d), and the position of the median x and y values of the $n(n-1)/2 = 190$ expected intersections was thus obtained. The great majority of intersections are tightly grouped into the MD–lever junction, reinforcing the observation that flexibility in the head is mainly a hinge at this site. Superposition of the ScS1 apo crystal structure shows that the location where bending is focused is indeed at the junction between the MD and the lever (Fig. 5e) at about heavy chain residue 772. This indicates that, within the error of our estimate, the lever flexes in the pliant region (residues 774–781) previously described in myosin-2 between the converter and ELC [15,17,29] and predicted to be a source of elasticity in the cross-bridge [14].

Measurement and comparison of lever stiffness

For a thermally excited torsion spring, such as the hinge between the MD and the lever, the torsion spring constant, κ, is inversely related to the variance in lever angle, σ^2, through the Equipartition theorem as $\kappa = k_B T/\sigma^2$, where k_B is Boltzmann's constant and

Table 1. Lever angle and bending stiffness of the four S1 types

S1 type	MD class	Mean lever angle (°)	Lever angle SD (°)	Torsion spring constant (pN·nm/rad^2)	Cantilever-type stiffness (pN/nm)
RbS1	32	−2.74	21.82	27.85	0.435
RbS1	33	−3.40	23.58	23.85	0.373
RbS1	35	−2.72	22.73	25.67	0.401
RbS1	36	−2.31	22.94	25.20	0.394
RbS1	64	2.90	21.95	27.53	0.430
RbS1	67	−0.65	24.12	22.79	0.356
RbS1	76	−0.54	23.07	24.92	0.389
RbS1	84	0.82	24.42	22.23	0.347
ScS1	32	−7.66	25.99	19.64	0.307
ScS1	33	−6.11	24.64	21.84	0.341
ScS1	35	−12.61	26.27	19.21	0.300
ScS1	36	−5.36	25.75	20.00	0.313
ScS1	64	−2.12	26.21	19.31	0.302
ScS1	67	−10.76	25.14	20.99	0.328
ScS1	76	0.87	24.37	22.34	0.349
ScS1	84	2.26	23.00	25.06	0.392
CkS1	32	−2.86	25.22	20.86	0.326
CkS1	33	−4.46	28.26	16.60	0.259
CkS1	35	−6.76	26.78	18.49	0.289
CkS1	36	−1.66	26.45	18.96	0.296
CkS1	64	4.02	26.21	19.30	0.302
CkS1	67	−5.36	26.47	18.93	0.296
CkS1	76	4.58	25.25	20.80	0.325
CkS1	84	6.35	22.66	25.82	0.403
mCkS1	32	2.84	19.72	34.12	0.533
mCkS1	33	−3.74	23.02	25.04	0.391
mCkS1	35	−6.01	25.17	20.93	0.327
mCkS1	36	−1.11	22.37	26.50	0.414
mCkS1	64	6.00	21.19	29.53	0.461
mCkS1	67	1.81	22.09	27.18	0.425
mCkS1	76	4.68	21.33	29.14	0.455
mCkS1	84	4.22	20.87	30.46	0.476

MD class corresponds to the major classes shown in Fig. 3d. Mean lever angle and standard deviation (SD) are obtained from Gaussian fits to each group of particles. Torsion spring constant and cantilever-type stiffness are calculated as described in Experimental Procedures.

T is absolute temperature [30]. This constant was calculated for each type of S1 for each of the eight MD classes (Fig. 3d) using the standard deviation of the distribution of lever angles assigned to individual particles (e.g., see Fig. 4). For the most abundant MD class, κ is in the range 19–29 pN·nm/rad^2 for the four types of S1. The values for the other MD classes also lie close to this range (Table 1), including for MD class 35 that shows S1 in a different orientation, indicating that stiffness at the pliant region may be isotropic. The overall mean ± SD value for κ is 23.4 ± 4.2 pN·nm/rad^2.

A more useful representation of the torsion spring stiffness for comparison to the stiffness of crossbridges in muscle, or to single molecule studies such as those performed using the optical trap, is the apparent stiffness measured at the tip of the lever, considering it as a bending beam. This cantilever-type lever stiffness was calculated for each type of S1 for each of the eight MD classes (Fig. 3d) as described in Experimental Procedures (Table 1). There is no systematic difference in lever stiffness among the eight MD classes. The mean ± SD stiffness values across these classes are 0.39 ± 0.032 pN/nm for RbS1, 0.33 ± 0.031 pN/nm for ScS1, 0.31 ± 0.042 pN/nm for CkS1 and 0.44 ± 0.062 pN/nm for mCkS1. Although some of these mean values are statistically different from one another, the differences are small. They could derive from differences between the S1 types in the amino acid sequence in the pliant region that could affect its stability or could arise merely from small systematic differences in specimen preparation. The overall average lever stiffness estimate is 0.37 ± 0.065 pN/nm.

Comparison of crystal structures of S1 to EM class averages

It is clear from Fig. 5e that the crystal structure of apo ScS1 can be oriented to fit well into a class average of the combined S1 data that is in the central (unstrained) region of the spread of lever angle. To test whether this was true for each S1 type taken separately, we compared a set of density projections covering all orientations of both ScS1 and mCkS1 crystal structures by cross-correlation against class

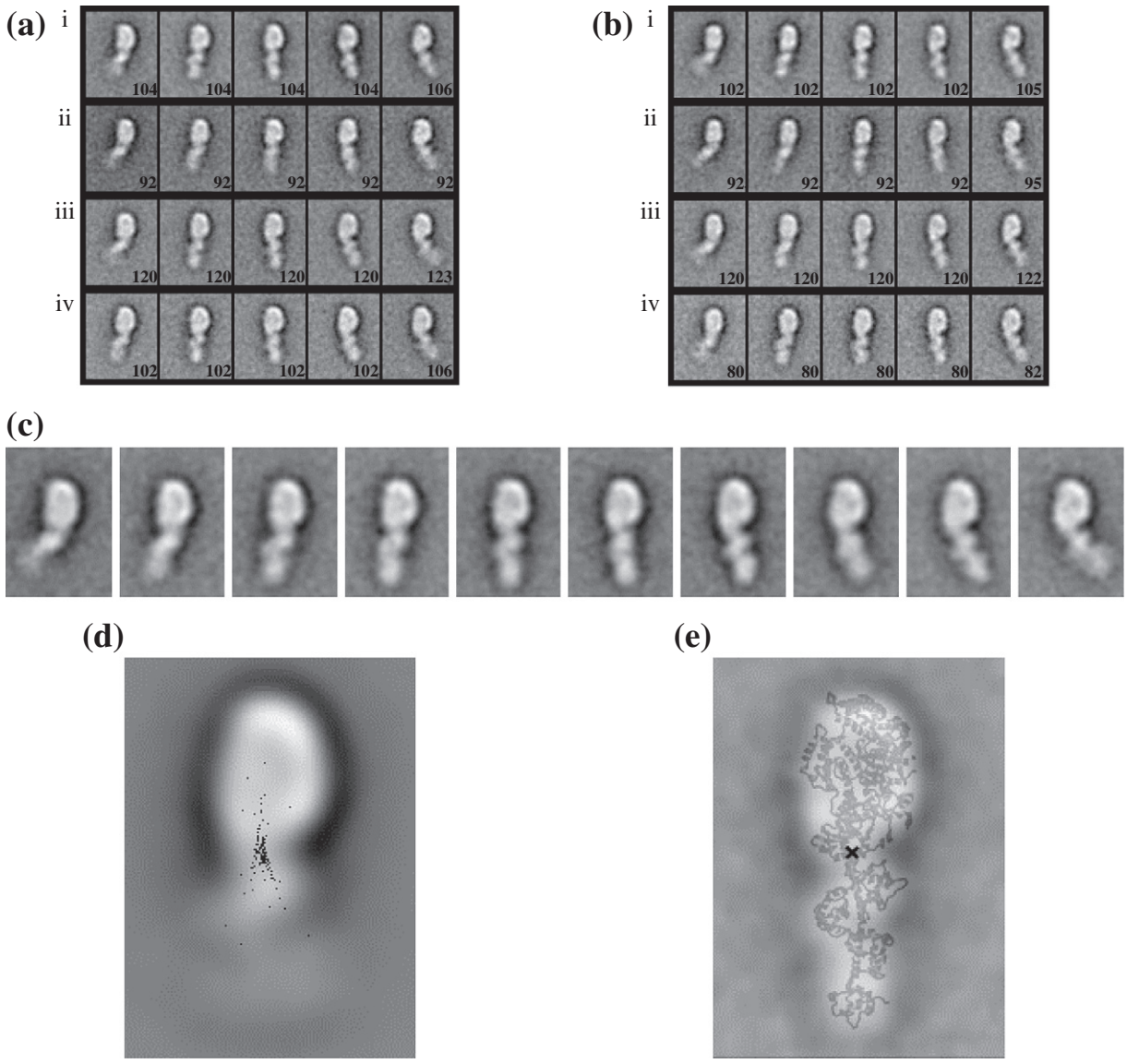

Fig. 5. Lever angle variation within a single MD orientation.(a and b) MD classes 64 and 36, respectively, as shown in Fig. 3d. Within each panel, an MD class is separated into four rows comprising the four types of S1 [(i), RbS1; (ii), ScS1; (iii), CkS1; (iv), mCkS1], and each row contains five image averages, each made using one-fifth of the particles after sorting them into order of increasing lever angle (i.e., the leftmost panel of a row contains the 20% of the particles with the lever angled most to the left). Number of particles in each average is shown at lower right. Side length of all image panels is 31.2 nm. (c) Data from MD class 64 (all S1 types combined) regrouped into 10 equal-sized classes of ascending lever angle. (d) Scatter plot of the intersections between lines drawn through the lever long axis of the MD class 64 after regrouping particles into 20 equal-sized classes of ascending lever angle (there are n(n–1)/2 = 190 such intersections), as also used to make SI Movie 1. The scatter plot is superposed on the global average of class 64. (e) The median point of the scatter plot (black cross) superposed on apo ScS1 crystal structure (PDB ID: 1SR6; grey ribbons) itself oriented to best match the appearance of the fifth class in (c) (faded, in background).

averages of the four S1 types in each of the eight populous MD appearances (Fig. 3d). Such a comparison cannot be rigorous because the EM data are dominated by negative stain that is absent from the crystal structures (discussed in Ref. [18]). Nevertheless, for the averages that include the centre of the angular spread (e.g., the central columns in Fig. 5a and b), all 32 comparisons showed that the ScS1 structure was the closer fit, even to the mCkS1 data. This is principally due to the smaller angle between motor and lever long axes in the ScS1 structure yielding a closer match to the rather straight S1 shape of all S1 types at the centre of their lever angle distributions (Fig. 6).

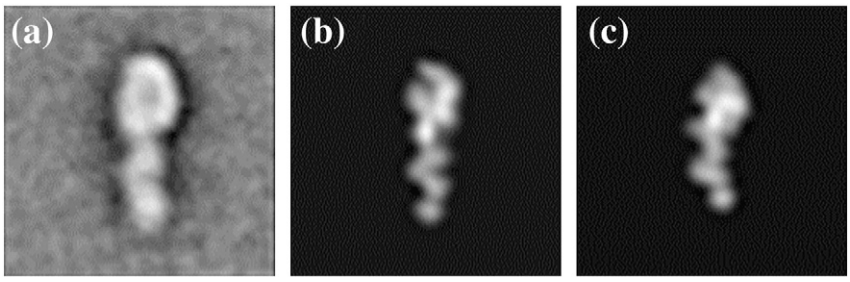

Fig. 6. Example of projection matching of S1 crystal structures to EM class averages.(a) Image average of RbS1 from MD class 64, using 20% of images closest to the mean lever angle (central panel from Fig. 5a-i). (b) 2D projection of apo ScS1 crystal structure density that best matches (a); cross-correlation coefficient, 0.681. (c) 2D projection of apo mCkS1 crystal structure density that best matches (a); cross-correlation coefficient, 0.636. 2D projection densities were inverted so that high density is pale, zero density is black, to better match the EM image. Side length of all panels is 31.2 nm.

Discussion

We have extended earlier work on intact muscle myosin molecules [18] by finding that isolated myosin-2 heads retaining either one light chain or both light chains (total mass, 110–130 kDa) are amenable to quantitative analysis through negative-stain EM and single particle image processing. These combined techniques produce class averages in which individual subdomains of the myosin motor and light chains can be identified and sites and extents of flexibility can be identified. S1s from myosin-6 [31] and myosin-18A [32] have also been studied in this way. Interestingly, myosin-6 typically adsorbed to the carbon film also in the head-in-profile view we see, but facing the opposite way; that is, the other side of the head is adsorbed as compared with myosin-2 and myosin-18A (and also myosin-5 heads in a two-headed construct [24]).

All S1 types investigated display a variety of appearances when the images are grouped and averaged. From the appearance of the MDs, this variety is owing to some variation in the orientation by which each S1 molecule binds to the carbon substrate but, principally, to conformational variability within a given population of molecules. The typical appearance of all types was similar at this resolution to crystal structures of nucleotide-free ScS1, in which the long axis of the MD is approximately parallel to the long axis of the lever, rather than to the crystal structure of mCkS1, which is more bent. Interestingly, while this was true in the case of class averages from unmodified CkS1, it remained true even when the protein had been methylated so as to reproduce the material used to determine the first S1 crystal structure [10]. This suggests that the mCkS1 crystal structure represents just one of a range of conformations available to the molecule and that other conformations, more closely resembling those seen in the ScS1 crystal structures, are more common in solution. Conversely, some class averages of every S1 type are as bent as the mCkS1 crystal structure, which suggests that this bent conformation is part of the range of conformations naturally available to the molecule but that only a small proportion of the molecules adopt this conformation at any given time (Fig. 5). The earlier study of the heads of intact myosin-2 [18] also found the typical shape was less bent than the mCkS1 crystal structure, but at that time, the ScS1 structure had not been determined.

The distributions of lever angles in the four S1 types investigated were remarkably similar, including the mean lever angle (Fig. 4 and Table 1). The differences between them are small compared to the large differences seen in the lever angle when comparing the crystal structures of ScS1 and mCkS1 [10,28]. This contrasts with data from S1s bound to F-actin, for which differences in S1 shape between S1 types have been detected, and the CkS1 lever was more curved than that of insect flight muscle S1 [33,34].

Overall, the range of appearances of the S1 molecule seen in this study includes conformations similar to those seen by X-ray crystallography while also suggesting a continuum of conformations around a single, optimum conformation (similar to that represented by the global average). This variation is most likely to be due to thermally excited flexibility within the molecule rather than to large rearrangements of the subdomains of the motor relative to each other to produce a series of discrete conformations. This conclusion is supported by the fact that lever angles are distributed as a Gaussian around a single peak rather than over multiple peaks, as would be the case if the molecule were adopting distinct conformations. It is possible that diversity of appearances can also have contributions from adsorption of the S1 onto the carbon film and the surface tension forces during drying of the film of stain. By working with just the heads rather than whole myosin molecules, we have minimised the shearing forces that could arise when different parts of a single molecule adsorb at different times or the distortion of a large-scale three-dimensional (3D) structure when it dries down

onto the two-dimensional (2D) film. In general, drying forces are expected to act perpendicular to the plane of the carbon film, whereas the flexibility we observe is in the plane of the film. The good match between the global image average of apo ScS1 and the apo ScS1 crystal structure suggests that there is little systematic distortion, while the similarity of the torsional stiffness to that of molecules in solution (see below) suggests that the flexibility observed is not induced by specimen preparation.

By classifying images based on features in the MD, and then reclassifying within each MD class based on features in the lever, we have identified the major site of flexibility to be the pliant region of the myosin heavy chain between the converter of the MD and the ELC of the lever [14], rather than, for instance, a curvature along the whole lever or the fulcrum within the MD that is associated with the lever swing of the power stroke [15,35]. All myosin-2s that have been studied, including scallop striated muscle myosin, show pronounced bending at this pliant region in forming the specific heads-down relaxed conformation [17,20,36–38], even though in ScS1 the crystal structures in various states all have little flexion at this site. The fact that the switch between heads-down and active conformations is controlled merely by relatively weak binding of Ca^{2+} to scallop ELC [39] or by phosphorylation of the RLC in many other myosins indicates that this distortion requires little energy. The specific heads-down conformation of myosin-2 is formed *in vivo* in the presence of ATP, which favours adoption of the pre-power stroke conformation of the MD (also known as the post-recovery stroke conformation) [24], in which the converter domain is in a markedly different location with respect to the rest of the MD. It will be of interest to determine whether flexion in the pliant region has different characteristics in the pre-power stroke MD conformation.

S1 from several sources crystallised in the absence of nucleotide has shown two distinct conformations known as the rigor-like and post-rigor states (see Ref. [16] and references therein); thus, it is of interest to examine whether our data distinguish which conformation of S1 predominates under our solution conditions. *In vivo*, the post-rigor conformation would require binding of ATP to S1 to force the structural changes that weaken the strong rigor actomyosin bond, but for isolated S1, a sulfate ion in the nucleotide pocket can suffice to induce a similar change. For ScS1, the rigor-like and post-rigor states are represented by PDB IDs 2OS8 and 1SR6, respectively. Comparisons between the two scallop conformers show that there are no large-scale shape differences that would allow us to discriminate between the conformers. However, normal mode analysis of the transition between the two structures in myosin-5 S1 has suggested that flexibility in the converter region differs markedly, such that flexion occurs at the pliant region in the rigor-like structure whereas flexion is instead at the converter–SH1 helix junction within the MD in the post-rigor structure [40]. Since the EM data show that the fulcrum of lever flexibility lies in the pliant region, and not within the MD, it appears that, under our conditions, muscle S1 is predominantly in the rigor-like conformation, as should perhaps be expected since our solution lacks sulfate.

Our calculation of the torsion spring constant at the MD–lever junction in apo S1 (~ 23 pN·nm/rad^2) is remarkably similar to the value (≥ 20 pN·nm/rad^2) found for apo myosin-5 [41]. That value was obtained by tethering the lever to a surface and observing through the light microscope the time-varying position of beads attached to the MD, and it was hardly changed when ATP was present. Our value is about 2 orders of magnitude higher than that derived from measuring the spread of angles between fluorescent actin filaments attached to the two heads of scallop heavy meromyosin molecules in solution (0.52 pN·nm/rad^2 at low calcium conditions and 0.17 pN·nm/rad^2 at high calcium) [42], though the stiffness being observed, in that case, may be that of the junction of each head with the tail, which is expected to be low [43].

The majority of our data on lever flexibility refers to molecules in which the MD is seen in the head-in-profile view; thus, it is natural to wonder how that would translate into axial and azimuthal lever movement if the MD were strongly attached to the actin filament. Inspection of such S1-decorated actin [44] shows that the head-in-profile view is obtained by viewing the actin filament obliquely from the barbed end at an angle of $\sim 45°$. Therefore, if flexion of the lever occurred only in that plane, it would be divided roughly equally between azimuthal and axial components, and thus, the apparent axial stiffness would be about 1.4× higher than that we report. However, we find the same lever stiffness for an MD class that is differently oriented, which suggests that flexion at the pliant region is isotropic, and thus, that the axial stiffness is likely to be the same as we have measured.

The torsional spring at the MD–lever junction produces a stiffness for displacement of the tip of the myosin-2 lever of 0.37 pN/nm. The value obtained is much lower than recent determinations of the stiffness of myosin-2 heads attached to actin, either as single molecules in the optical trap or as crossbridges in muscle [45]. Because this stiffness, when derived from a torsional stiffness, is inversely proportional to the square of lever length then, other things being equal, the stiffness of myosin-5 with its 3-fold longer lever is expected to be one-ninth of this value, that is, 0.041 pN/nm, which is much lower than the estimate obtained from heads bound to actin (0.2 pN/nm) [46] and would seem to suggest an

impossibly large distortion (~60 nm) near the 2.5 pN stall force of myosin-5.

How might the low stiffness of the pliant region be reconciled with the higher stiffness of myosin heads moving along their actin tracks? Evidence suggests that the answer may be that strong binding to actin stiffens the head. 3D reconstructions of actin filaments saturated with myosin heads from various sources [33,47–49] consistently show strong features in the levers and a lack of contact between them, out to high radius from the actin, implying that the lever maintains a rather fixed geometric relationship to the actin helix; that is, it is not flexing at the MD–lever junction. NMR studies of myosin heads found over 20% of mobile structure and all this became immobile upon binding actin [50]. A high proportion of rapid backbone amide hydrogen exchange in S1 is quenched by actin binding [51]. In contrast, flexibility is implied by formation of the specific heads-down structure in shutdown myosin-2; furthermore, our measurement of flexibility in isolated myosin heads implies a standard deviation of the tip of the myosin-2 lever of about 3.5 nm, which would greatly smear out the density in 3D reconstructions. An attractive hypothesis is that easy flexibility at the MD–lever junction allows the myosin head great freedom to locate an actin binding site, after which this junction stiffens in an allosteric response to the formation of a strong interface between the MD and actin, and thus contributes to force generation.

Experimental Procedures

Proteins

Rabbit skeletal myosin was prepared from rabbit dorsal back and hind leg muscle using a method based on Ref. [52]. Myosin was digested with papain to produce RbS1 with both ELC and RLC [53]. RbS1 containing only the A1 ELC was prepared by chymotryptic digestion [26]. Scallop myosin was prepared from the striated adductor muscle of *Pecten maximus* by ammonium sulfate fractionation (Ref. [54] as modified in Ref. [55]). ScS1 was prepared from the purified myosin by papain digestion and further purified by ammonium sulfate fractionation (Ref. [56] with modifications described in Ref. [57]). Purified CkS1, prepared using papain, was a kind gift of Dr. Ivan Rayment. It was reductively methylated [58], and amino acid analysis (Alta Bioscience) showed that 97.4% of lysines had been methylated, as expected [25].

In order to remove inactive heads from each protein preparation (apart from mCkS1, which is all inactive [25]), we used a method based on Ref. [59]. The S1 was first centrifuged with actin, and the supernatant was removed, to select for S1 that had actin-binding capability. The actomyosin pellet was then resuspended in ATP-containing buffer and centrifuged again. The supernatant was collected and all S1 in the supernatant that had been released from actin by the presence of ATP was considered to be fully active. ATP was then removed by dialysis against an apyrase-containing buffer [at least 100 ml containing 2.5 units apyrase (Sigma A6535)] or using a NAP-5 desalting column (Amersham Biosciences). Samples were also mixed with 0.5 units/ml apyrase (Sigma A6535) on ice for 15 min prior to use to ensure complete removal of ATP and ADP. The particular preparation of apyrase used had equal rates of conversion for ATP to ADP and for ADP to AMP. One unit of the enzyme is defined as the amount that liberates 1.0 μmol of inorganic phosphate from ATP or ADP per minute at pH 6.5 and 30 °C, and this rate drops 10-fold in ice (H. D. White, personal communication).

Electron microscopy

Thawed proteins were diluted with 25 mM KCl, 10 mM 3-(N-morpholino)propanesulfonic acid, 2 mM $MgCl_2$ and 1 mM ethylene glycol bis(β-aminoethyl ether) *N,N,N′,N′*-tetraacetic acid (pH 7.0 at 20 °C) then applied to grids with a thin carbon film and negatively stained with 1% aqueous uranyl acetate as described previously [60] but without using a buffer rinse prior to staining. Final protein concentrations were 50–100 nM. Micrographs were recorded on film using a Jeol 1200EX microscope at moderate dose (~100 e/$Å^2$)

Image processing of individual S1 types

Micrographs were digitised at a pixel size corresponding to 0.52 nm in the specimen and imported into the SPIDER software suite, as described previously [11]. Individual heads were selected manually by a mouse click midway along the molecule and windowed out of the micrographs to form a series of individual images. These were then aligned by reference-free methods. K-means (rather than hierarchical) clustering was used to divide the dataset into groups for averaging in the initial classification as this method is most useful for revealing diversity within the dataset by subdividing a dataset into groups of approximately equal size [61]. A mask was drawn around the whole molecule (using the global variance image as a guide) to reduce the effect of background noise in the classification, as described previously [11].

Image processing of the pooled datasets

To allow a comparison between different S1s, we pooled datasets from four different S1s. To reduce bias, we truncated the RbS1 and ScS1 datasets to be the same size (4,619 particles) as the CkS1 dataset, giving a combined dataset of 17,307 particles. The

data were aligned by reference-free methods. The aligned images were classified into 400 classes using K-means clustering and a whole molecule mask. From the 400 classes, 309 class averages that showed a clearly identifiable MD and lever were selected (containing 13,176 particles), and 91 classes were discarded (generally having poor staining) in which both MD and lever could not easily be identified. Using the 309 class average images, we then aligned the motors in the images such that the long axis of the motor was approximately vertical within the window. This was performed using a model image created using the global average from the previous alignment, shifted such that the MD was centrally located within the window and rotated so that its long axis was vertical with respect to the window. Class averages rather than individual images were aligned in this way since we found that the high noise in individual images precluded the alignment of such a relatively small and roughly circular region (the MD alone is only ~80 kDa). The parameters from the whole molecule alignment and the MD alignment were combined into a single set of shift and rotation vectors, which were then applied to the original windowed images to produce a stack of images in which all molecules were aligned with their MD approximately vertical within the window.

The global variance image from the MD-aligned image stack was used to draw a mask around the MD. The stack of individual images was classified into 100 classes based on the pixels within the mask, using hierarchical ascendant classification to create large classes of the most abundant MD appearances. A second mask was created using the global variance image to draw around the region encompassing all possible lever positions and excluding the MD. This was performed iteratively to find the tightest possible lever mask that did not exclude any lever positions. The stack of individual images was classified into 200 lever classes based on the pixels within the mask, using K-means clustering to obtain classes of similar size.

For each of the 200 lever classes, to calculate the angle of the lever relative to the vertical axis of the image window, and thus relative to the vertically-aligned MD, a point deemed to best represent the tip of the lever was selected. Using this pixel location together with the pixel location of the point where the lever joins the MD (marked in the global average image of MD-aligned images), we calculated the lever angle (Fig. 3f).

The particles in each MD class were separated into four subclasses, one for each S1 type. Each of these subclasses was then divided into five bins, based on ascending lever angles assigned to the particles such that the first bin contained the 20% of images from that type of S1 with the lowest lever angles and the next bin contained the next 20% of lowest lever angles and so on. The average image was then calculated from the contents of each bin.

Calculation of lever stiffness

The torsion spring constant of the lever of each species of S1 was calculated using $\kappa = k_B T/\sigma^2$, where κ is the torsion spring constant ($N \cdot m/rad^2$), k_B is the Boltzmann constant (1.381×10^{-23} N·m/K), T is the absolute temperature (293 K in all cases) and σ^2 is the variance of the lever displacement (rad^2) [30]. To convert torsion spring constant to apparent cantilever stiffness (k), we took the energy for rotation of the lever through angle θ to be equal to the energy required to bend the lever such that its tip is displaced by the same distance (x) as produced by the angular rotation. Thus, $kx^2/2 = \kappa\theta^2/2$. For a lever of length L, $x = L\sin\theta$. Hence, for small displacements, for which $\sin\theta \approx \theta$, $k = \kappa/L^2$. L was taken to be 8 nm for all S1s.

Comparison to crystal structures

To allow comparison of EM averages with crystal structures of myosin-2 S1, we made low-resolution 2D projections of nucleotide-free structures of ScS1 (PDB ID: 1DFK) and mCkS1 (PDB ID: 2MYS). The structure file 1DFK contains only β-carbons for the side chains; these were completed using Swiss PDB Viewer. 2MYS.pdb contains only α-carbons of the light chains; we used a structure file containing all atoms for these chains, kindly supplied by Dr. Ivan Rayment.

PDB files were converted to 3D SPIDER volumes. An angular document file containing three Euler angles defining quasi-evenly spaced projection directions was created with an angular step of 5º in θ and was used to produce a set of 799 2D projections from each of the two 3D structure files that represented one hemisphere of projections. Each EM class average was then compared to each of the two sets of projection images, as well as to their mirror images that represent the other hemisphere. Cross-correlation score was used to determine the optimum rotation and translation of each projection, and the projection with the highest score was taken to be the best match of each crystal structure to that EM class average.

Although the EM data were collected in the absence of calcium and the ScS1 crystal structure data to which they were compared were collected in the presence of calcium, crystallographic data indicate that the effect of calcium on the overall conformation of ScS1 is likely to be small [16,62].

Supplementary data to this article can be found online at http://dx.doi.org/10.1016/j.jmb.2013.11.028.

Acknowledgements

We thank Drs. Hitesh Patel, Howard White and Ivan Rayment for supplying protein and for helpful

discussions. This work was funded in part by a Biotechnology and Biological Sciences Research Council postgraduate studentship to N.B., a Wellcome Trust studentship to DJR (086778/Z/08/Z) and by NHLBI intramural funds (HL001786) to James Sellers.

Received 1 October 2013;
Received in revised form 25 November 2013;
Accepted 29 November 2013
Available online 9 December 2013

Keywords:
electron microscopy;
image processing;
stiffness;
pliant region;
crossbridge

† Present address: N. Billington, Laboratory of Molecular Physiology, NHLBI, National Institutes of Health, Bethesda, MD 20892-8015, USA.

Abbreviations used:
S1, myosin subfragment-1; CkS1, chicken skeletal muscle myosin subfragment-1; mCkS1, methylated chicken skeletal muscle myosin subfragment-1; RbS1, rabbit skeletal muscle myosin subfragment-1; ScS1, scallop cross-striated adductor muscle myosin subfragment-1; MD, motor domain; ELC, essential light chain; RLC, regulatory light chain; EM, electron microscopy; 3D, three-dimensional; 2D, two-dimensional.

References

[1] Offer G, Ranatunga KW. Crossbridge and filament compliance in muscle: implications for tension generation and lever arm swing. J Muscle Res Cell Motil 2010;31:245–65.
[2] Offer G, Ranatunga KW. Stiffness and number of cross-bridges attached in active frog muscle: a reply to Professor Lombardi. J Muscle Res Cell Motil 2011;32:5–6.
[3] Offer G, Ranatunga KW. A cross-bridge cycle with two tension-generating steps simulates skeletal muscle mechanics. Biophys J 2013;105:928–40.
[4] Lombardi V. Clarification in relation to the review paper "Crossbridge and filament compliance in muscle: implications for tension generation and lever arm swing". J Muscle Res Cell Motil 2011;32:3.
[5] Cooke R. The mechanism of muscle contraction. CRC Crit Rev Biochem 1986;21:53–118.
[6] Odronitz F, Kollmar M. Drawing the tree of eukaryotic life based on the analysis of 2,269 manually annotated myosins from 328 species. Genome Biol 2007;8:R196.
[7] Berg JS, Powell BC, Cheney RE. A millennial myosin census. Mol Biol Cell 2001;12:780–94.
[8] Spudich J. How molecular motors work. Nature 1994;372:515–8.
[9] Cheney RE, Mooseker MS. Unconventional myosins. Curr Opin Cell Biol 1992;4:27–35.
[10] Rayment I, Rypniewski WR, Schmidt-Bäse K, Smith R, Tomchick DR, Benning MM, et al. Three-dimensional structure of myosin subfragment-1: a molecular motor. Science 1993;261:50–8.
[11] Burgess SA, Walker ML, Thirumurugan K, Trinick J, Knight PJ. Use of negative stain and single-particle image processing to explore dynamic properties of flexible macromolecules. J Struct Biol 2004;147:247–58.
[12] Liu J, Reedy MC, Goldman YE, Franzini-Armstrong C, Sasaki H, Tregear RT, et al. Electron tomography of fast frozen, stretched rigor fibers reveals elastic distortions in the myosin crossbridges. J Struct Biol 2004;147:268–82.
[13] Brown JH, Kumar VSS, O'Neall-Hennessey E, Reshetnikova L, Robinson H, Nguyen-McCarty M, et al. Visualizing key hinges and a potential major source of compliance in the lever arm of myosin. Proc Natl Acad Sci USA 2011;108:114–9.
[14] Houdusse A, Szent-Györgyi AG, Cohen C. Three conformational states of scallop myosin S1. Proc Natl Acad Sci USA 2000;97:11238–43.
[15] Dominguez R, Freyzon Y, Trybus KM, Cohen C. Crystal structure of a vertebrate smooth muscle myosin motor domain and its complex with the essential light chain: visualization of the pre-power stroke state. Cell 1998;94:559–71.
[16] Yang YT, Gourinath S, Kovács M, Nyitray L, Reutzel R, Himmel DM, et al. Rigor-like structures from muscle myosins reveal key mechanical elements in the transduction pathways of this allosteric motor. Structure 2007;15:553–64.
[17] Jung HS, Burgess SA, Billington N, Colegrave M, Patel H, Chalovich JM, et al. Conservation of the regulated structure of folded myosin 2 in species separated by at least 600 million years of independent evolution. Proc Natl Acad Sci USA 2008;105:6022–6.
[18] Burgess SA, Walker ML, White HD, Trinick J. Flexibility within myosin heads revealed by negative stain and single-particle analysis. J Cell Biol 1997;139:675–81.
[19] Kaya M, Higuchi H. Nonlinear elasticity and an 8-nm working stroke of single myosin molecules in myofilaments. Science 2010;329:686–9.
[20] Burgess SA, Yu S, Walker ML, Hawkins RJ, Chalovich JM, Knight PJ. Structures of smooth muscle myosin and heavy meromyosin in the folded, shutdown state. J Mol Biol 2007;372:1165–78.
[21] Hvidt S, Nestler FHM, Greaser ML, Ferry JD. Flexibility of myosin rod determined from dilute solution viscoelastic measurements. Biochemistry 1982;21:4064–73.
[22] Howard J. Mechanics of motor proteins and the cytoskeleton. Sunderland, MA: Sinauer Associates, Inc.; 2001.
[23] Walker M, Trinick J. Visualization of domains in native and nucleotide-trapped myosin heads by negative staining. J Muscle Res Cell Motil 1988;9:359–66.
[24] Burgess S, Walker M, Wang F, Seller JR, White HD, Knight PJ, et al. The prepower stroke conformation of myosin V. J Cell Biol 2002;159:983–91.

[25] White HD, Rayment I. Kinetic characterization of reductively methylated myosin subfragment 1. Biochemistry 1993;32:9859–65.
[26] Weeds AG, Taylor RS. Separation of subfragment-1 isoenzymes from rabbit skeletal muscle myosin. Nature 1975;257:54–6.
[27] Knight P, Trinick J. Structure of the myosin projections on native thick filaments from vertebrate skeletal muscle. J Mol Biol 1984;177:461–82.
[28] Himmel DM, Gourinath S, Reshetnikova L, Shen Y, Szent-Györgyi AG, Cohen C. Crystallographic findings on the internally uncoupled and near-rigor states of myosin: further insights into the mechanics of the motor. Proc Natl Acad Sci USA 2002;99:12645–50.
[29] Gourinath S, Himmel DM, Brown JH, Reshetnikova L, Szent-Györgyi AG, Cohen C. Crystal structure of scallop myosin S1 in the pre-power stroke state to 2.6 Å resolution: flexibility and function in the head. Structure 2003;11:1621–7.
[30] Reif F. Fundamentals of statistical and thermal physics. New York, NY: McGraw-Hill; 1956.
[31] Song CF, Sader K, White H, Kendrick-Jones J, Trinick J. Nucleotide-dependent shape changes in the reverse direction motor, myosin VI. Biophys J 2010;99:3336–44.
[32] Guzik-Lendrum S, Heissler SM, Billington N, Takagi Y, Yang Y, Knight PJ, et al. Mammalian myosin-18A, a highly divergent myosin. J Biol Chem 2013;288:9532–48.
[33] Littlefield KP, Ward AB, Chappie JS, Reedy MK, Bernstein SI, Milligan RA, et al. Similarities and differences between frozen-hydrated, rigor acto-S1 complexes of insect flight and chicken skeletal muscles. J Mol Biol 2008;381:519–28.
[34] Volkmann N, Ouyang G, Trybus KM, DeRosier DJ, Lowey S, Hanein D. Myosin isoforms show unique conformations in the actin-bound state. Proc Natl Acad Sci USA 2003;100:3227–32.
[35] Uyeda TQP, Abramson PD, Spudich JA. The neck region of the myosin motor domain acts as a lever arm to generate movement. Proc Natl Acad Sci USA 1996;93:4459–64.
[36] Wendt T, Taylor D, Trybus KM, Taylor K. Three-dimensional image reconstruction of dephosphorylated smooth muscle heavy meromyosin reveals asymmetry in the interaction between myosin heads and placement of subfragment 2. Proc Natl Acad Sci USA 2001;98:4361–6.
[37] Woodhead JL, Zhao FQ, Craig R, Egelman EH, Alamo L, Padrón R. Atomic model of a myosin filament in the relaxed state. Nature 2005;436:1195–9.
[38] Jung HS, Komatsu S, Ikebe M, Craig R. Head-head and head-tail interaction: a general mechanism for switching off myosin II activity in cells. Mol Biol Cell 2008;19:3234–42.
[39] Xie X, Harrison DH, Schlichting I, Sweet RM, Kalabokis VN, Szent-Györgyi AG, et al. Structure of the regulatory domain of scallop myosin at 2.8 Å resolution. Nature 1994;368:306–12.
[40] Cecchini M, Houdusse A, Karplus M. Allosteric communication in myosin V: from small conformational changes to large directed movements. PLoS Comput Biol 2008;4:e1000129.
[41] Shiroguchi K, Chin HF, Hannemann DE, Muneyuki E, De La Cruz EM, Kinosita K. Direct observation of the myosin Va recovery stroke that contributes to unidirectional stepping along actin. PLoS Biol 2011;9:e1001031.
[42] Azzu V, Yadin D, Patel H, Fraternali F, Chantler PD, Molloy JE. Calcium regulates scallop muscle by changing myosin flexibility. Eur Biophys J 2006;35:302–12.
[43] Elliott A, Offer G. Shape and flexibility of the myosin molecule. J Mol Biol 1978;123:505–19.
[44] Behrmann E, Muller M, Penczek PA, Mannherz HG, Manstein DJ, Raunser S. Structure of the rigor actin-tropomyosin-myosin complex. Cell 2012;150:327–38.
[45] Kaya M, Higuchi H. Stiffness, working stroke, and force of single-myosin molecules in skeletal muscle: elucidation of these mechanical properties via nonlinear elasticity evaluation. Cell Mol Life Sci 2013;70:4275–92.
[46] Veigel C, Wang F, Bartoo ML, Sellers JR, Molloy JE. The gated gait of the processive molecular motor, myosin V. Nat Cell Biol 2002;4:59–65.
[47] Jontes JD, Milligan RA. Brush border myosin-I structure and ADP-dependent conformational changes revealed by cryoelectron microscopy and image analysis. J Cell Biol 1997;139:683–93.
[48] Holmes KC, Angert I, Kull FJ, Jahn W, Schroder RR. Electron cryo-microscopy shows how strong binding of myosin to actin releases nucleotide. Nature 2003;425:423–7.
[49] Volkmann N, Liu HJ, Hazelwood L, Krementsova EB, Lowey S, Trybus KM, et al. The structural basis of myosin V processive movement as revealed by electron cryomicroscopy. Mol Cell 2005;19:595–605.
[50] Highsmith S, Akasaka K, Konrad M, Goody R, Holmes K, Wade-Jardetzky N, et al. Internal motions in myosin. Biochemistry 1979;18:4238–44.
[51] Prince HP, Trayer HR, Henry GD, Trayer IP, Dalgarno DC, Levine BA, et al. Proton nuclear-magnetic-resonance spectroscopy of myosin subfragment 1 isoenzymes. Eur J Biochem 1981;121:213–9.
[52] Perry SV. Myosin adenosine triphosphatase. Methods Enzymol 1955;2:582–8.
[53] Margossian SS, Lowey S, Barshop B. Effect of DTNB light chain on the interaction of vertebrate skeletal myosin with actin. Nature 1975;258:163–6.
[54] Chantler PD, Szent-Györgyi AG. Spectroscopic studies on invertebrate myosins and light chains. Biochemistry 1978;17:5440–8.
[55] Patel H, Margossian SS, Chantler PD. Locking regulatory myosin in the off-state with trifluoperazine. J Biol Chem 2000;275:4880–8.
[56] Stafford WF, Szentkiralyi EM, Szent-Györgyi AG. Regulatory properties of single-headed fragments of scallop myosin. Biochemistry 1979;18:5273–80.
[57] Kalabokis VN, Szent-Györgyi AG. Cooperativity and regulation of scallop myosin and myosin fragments. Biochemistry 1997;36:15834–40.
[58] Rayment I. Reductive alkylation of lysine residues to alter crystallization properties of proteins. Methods Enzymol 1997;276:171–9.
[59] Yamashita H, Tyska MJ, Warshaw DM, Lowey S, Trybus KM. Functional consequences of mutations in the smooth muscle myosin heavy chain at sites implicated in familial hypertrophic cardiomyopathy. J Biol Chem 2000;275:28045–52.
[60] Walker M, Knight P, Trinick J. Negative staining of myosin molecules. J Mol Biol 1985;184:535–42.
[61] Frank J, Radermacher M, Penczek P, Zhu J, Li YH, Ladjadj M, et al. SPIDER and WEB: processing and visualization of images in 3D electron microscopy and related fields. J Struct Biol 1996;116:190–9.
[62] Himmel DM, Mui S, O'Neall-Hennessey E, Szent-Györgyi AG, Cohen C. The on–off switch in regulated myosins: different triggers but related mechanisms. J Mol Biol 2009;394:496–505.